PROCEEDINGS OF SCIENCE

ONLINE ICRC 2021
THE ASTROPARTICLE PHYSICS CONFERENCE
Berlin | Germany
37th International Cosmic Ray Conference
12–23 July 2021

Cosmic Ray Detection at the Murchison Radio-astronomy Observatory – a pathfinder for SKA-Low

Alexander Williamson,[a,*] **Clancy James,**[a] **Steven Tingay,**[a] **Justin Bray**[b] **and Tim Huege**[c,d]

[a] *Curtin University, International Centre for Radio Astronomy Research, Bentley, WA 6102, Australia,*
[b] *University of Manchester, JBCA, Dept. of Physics & Astronomy, Manchester M13 9PL, UK,*
[c] *Karlsruhe Institute of Technology, Institute for Astroparticle Physics (IAP), P.O. Box 3640, 76021 Karlsruhe, Germany*
[d] *Astrophysical Institute, Vrije Universiteit Brussel, Pleinlaan 2, 1050 Brussels, Belgium*
E-mail: alexander.williamson1@postgrad.curtin.edu.au, clancy.james@curtin.edu.au

We present the status of cosmic-ray detection activities at the Murchison Radio-astronomy Observatory. Using 128 antennas of the Murchison Widefield Array radio telescope in its extended configuration, we detect the radio emission from extensive air showers in the 122–154 MHz range at a rate of slightly less than once per hour, each with an approximate energy of 10^{17} eV. We have developed a bespoke filter inversion to obtain high-time-resolution data from this general-purpose astronomy instrument, and directly capture the radio signal. Our future plans include the implementation of a particle-triggered mode, and expanded operations with the low-frequency component of the Square Kilometre Array, which will have ~100,000 antennas deployed on the same site.

37th International Cosmic Ray Conference (ICRC 2021)
July 12th – 23rd, 2021
Online – Berlin, Germany

*Presenter

PoS(ICRC2021)325

1. Introduction

The radio-detection of cosmic rays has become increasingly popular in the digital era of radio astronomy [1]. In particular, LOFAR [2] has pioneered the use of a low-frequency radio telescope built primarily for imaging observations for cosmic ray detection, where the high antenna density yields a high degree of precision on individual events. More recently, OVRO-LWA have detected a sample of cosmic rays using a specialist observation mode [4]. In the long term, the High Energy Cosmic Particles focus group of the Square Kilometre Array (SKA) propose to use the SKA's low-frequency antenna for even high precision measurements [**?**].

The Murchison Widefield Array (MWA) is the SKA precursor at low frequencies [6]. Located in the Murchison radio-astronomy observatory in remote Western Australia, it consists of 256 16-antenna tiles, of which 128 are simultaneously capable of observing a 30.72 MHz bandwidth in the 70–350 MHz range. Covering a similar frequency range, and located on the same site, as SKA1-low, the MWA serves as an ideal instrument for making pathfinding observations for the SKA project, and for exploring the > 100 MHz emission of cosmic rays, where the ground pattern of cosmic ray emission remains relatively unexplored.

Here we describe our first observations and data processing in an initial search for cosmic ray events with the MWA. The MWA can be configured in one of two configurations — a compact configuration, used predominantly for Epoch of Reionisation observations; and an extended configuration, used for other imaging observations. For the period described in this work, the MWA has been in the extended configuration, with layout shown in Figure 5 (left).

2. Observations

In this first stage of the project, we have no real-time trigger to identify cosmic ray events. Thus, all data must be recorded and analysed offline. This meant that instead of observing in commensal mode, we performed targeted observations aimed at maximising the MWA's sensitivity to cosmic rays.

We chose to observe using coarse channels 96–119 (122.88–153.6 MHz). These gave a good compromise between being at the low-frequency end for greater comparability with prior radio observations of cosmic ray pulses, being near the MWA's peak sensitivity at 150 MHz, and avoiding strong RFI bands near 100 MHz. These channels also sit within Nyquist zones corresponding to either 30.72 MHz bandwidth or 40.96 MHz bandwidth, allowing for easy PFB inversion.

The MWA performs beamforming over all sixteen dipoles per tile at the analogue stage, providing instantaneous coverage to $\mathcal{O} \sim 600\,\mathrm{deg}^2$. It is this formed beam which is digitised and processed — voltages from individual MWA dipoles are not digitised, and are not recoverable. The MWA's sensitivity falls approximately as $\cos\theta_z$, where θ_z is the angle to the zenith. The cosmic ray signal however, which is dominated by geomagnetic emission [1], varies as $\sin\theta_B$, where θ_B is the angle to the local magnetic field. At the MRO, the field is approximately 55 μT, directed 60.2° above the horizon almost directly Northwards, [1] so that the radio signal will be strongest from cosmic rays arriving from an arc passing 60° South of the zenith. Therefore, we point the MWA

[1] https://www.ngdc.noaa.gov/geomag/calculators/magcalc.shtmligrfwmm

at approximately 30° South from the zenith, mid-way between the points of peak MWA sensitivity, and peak cosmic ray emission strength.

We recorded data using the MWA's Voltage Capture System (VCS) [7], which allows fine channel data from each antenna to be stored in a buffer at the MRO instead of being passed to the correlator. This generates 25.7 TB per hour of data, meaning that observations were limited to one hour at a time. Using the current link between the MRO and Perth, where offline processing is performed, buffer readout takes approximately two days.

The processing consisted of the following steps. Firstly, the data were inverted from dual linear polarisation complex data at a time–frequency resolution of 1 ms × 10 kHz to real data at a time resolution of approximately 16.3 ns over the full 30.72 MHz bandwidth. This involved synthesising data from both the fine and coarse MWA polyphase filterbanks as described in [8, 9].

The signals on each tile were then searched for voltages exceeding an RMS threshold of $6\,\sigma$ on either polarisation. After applying time corrections due to different cable delays, coincidences within a time window of 17 µs — corresponding to the light travel time across the MWA — involving four or more tiles were kept for further analysis. This yielded typically a few hundred events per hour, although some observations with strong RFI or tiles with spuriously high rates of $6\,\sigma$ events produced hourly rates in the thousands. A total of 26 hours of data have been taken in this mode, with two hours being affected by abnormally high rates. We expect those two hours to provide useful data, but for this initial analysis we exclude them. From the remaining 24 hr, we find 2819 candidate coincidences.

3. Data reduction

Cosmic ray events have unique characteristics that enable them to be identified against radio-frequency interference (RFI) and system noise. We use these criteria to successively reduce our candidate events and identify cosmic ray signatures for a final by-eye analysis.

3.1 Extent — the size of the ground pattern

The ground pattern of cosmic ray events is typically confined to an asymmetric annulus a few hundred metres in radius, although highly inclined events are projected up to a kilometre or more [1]. In contrast, random noise will show no preference for spatial structure, and far-field RFI (e.g. from satellites, aeroplanes, nearby roads etc.) will tend to be visible over most of the array.

For each event, we therefore calculate the maximum extent of contributing tiles in both the East–West and North–South direction, X_{EW} and X_{NS}. Figure 1 plots X_{EW} and X_{NS} for all 2819 candidates. Several features emerge. Firstly, there are a small number of strong RFI events detected in 20 or more tiles, which are extended over almost the entire array. Secondly, there is significant vertical and horizontal structure in Figure 1, reflecting the structure of the array. The data are dominated by four-fold coincident events, which are due primarily to random noise [9], but which may harbour genuine cosmic ray events.

In order to select for cosmic ray events, we consider only events with a geometric mean of extents, $(X_{\mathrm{EW}} X_{\mathrm{NS}})^{0.5}$, less than 1000 m. This excludes all but 285 candidates.

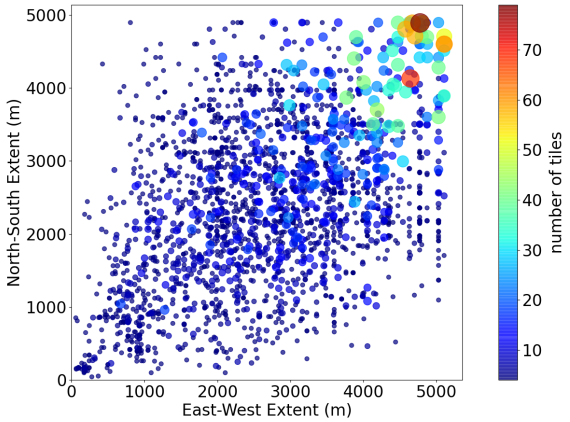

Figure 1: Extent of all candidates events for 24 hr of data. The extent is measured by taking the maximum East–West and North–South distances between triggering tiles, the number of which is shown by the colour/size of the points.

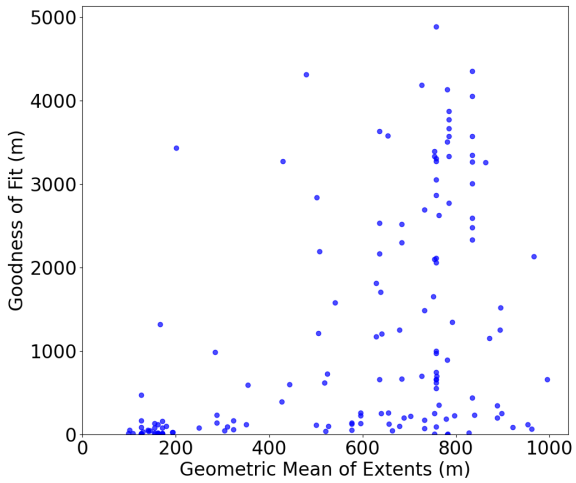

Figure 2: Goodness of fit (Eq. 1) to a planar wavefront as a function of the geometric mean of extents, $(X_{\mathrm{NS}} X_{\mathrm{EW}})^{0.5}$.

3.2 Expected arrival times

The radio wavefront of cosmic ray events is slightly curved, resembling a hyperboloid [3]. As a first approximation however, we begin by fitting a planar wavefront. The goodness of fit is defined as the square root of the minimised, reduced χ^2,

$$c \left[\frac{1}{N_{\mathrm{tiles}} - 3} \sum_{i}^{N_{\mathrm{tiles}}} (t_i - t_{\mathrm{fit}})^2 \right]^{0.5}, \tag{1}$$

where t_i is the time of peak voltage on tile i, and the normalisation accounts for the number of tiles, N_{tiles}, and the three fitted parameters (two velocity components and absolute time). It is translated to units of distance to allow easy comparison with the inter-tile distance.

This goodness-of-fit is plotted in Figure 2 for all events satisfying the extent criteria above. In Figure 1, many events having the same extent appear as a single point — here, these events

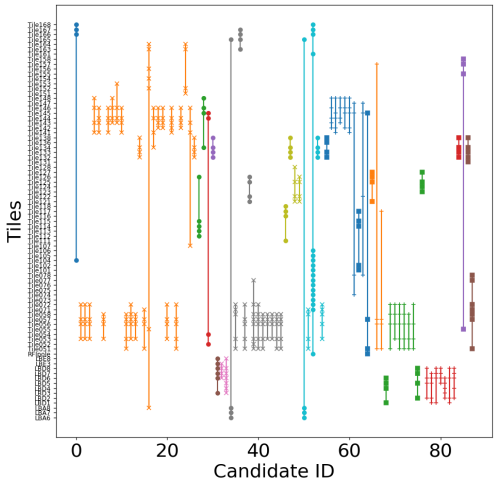

Figure 3: Events passing extent and goodness-of-fit cuts, showing tiles contributing to the coincidence (represented as symbols connected by a line). Those marked with '+' or 'x' are removed; those with solid squares or circles are kept.

become separated due to different goodnesses of fit. Events which are purely random will have times uniformly spread over a 17 µs interval, for a fit error of several km. This is clearly the case for many of the events, especially those at greater extents. There is however an excess of events with smaller fit errors that therefore likely represent real signals, cosmic ray or otherwise. We conservatively keep all events with a goodness of fit of 1000 m or less, to allow for potential timing errors. This leaves 88 remaining events.

3.3 Removal of repeating events

The remaining 81 events are displayed in Figure 3, which shows the tiles contributing to the coincidence. It is clear that many events show a repeated pattern, indicative of either a set of tiles with abnormally high rates, or of a (likely local) RFI source. We excise all events sharing three or more tiles within a single one-hour observation, leaving 21 candidates.

4. Visual inspection of events

Until this point, only the information of which and when tile voltages crossed the 6 σ threshold has been used. For these remaining events, the voltage sequences were extracted from the data and inspected by eye for consistency with an impulsive cosmic-ray-like signal, with findings below.

4.1 Time artefacts

The MWA's PFBs and associated inversion process has an impulse response function with artefacts offset at times corresponding to the PFB tap length, being 0.78125 µs for the coarse PFB and 100 µs for the fine filterbank [9]. For a true impulse, these artefacts should be at most 25% the amplitude of the primary pulse, depending on how the impulse aligns with the PFB filter coefficients.

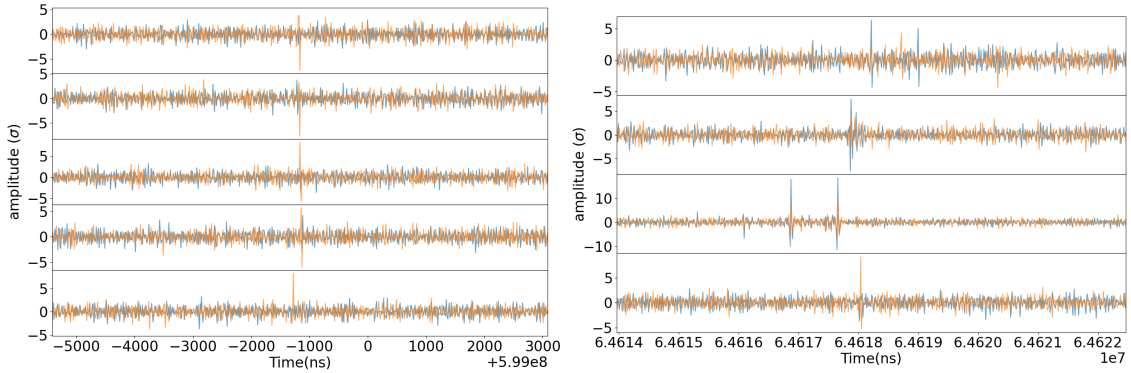

Figure 4: Traces showing reconstructed North-South (orange) and East-West (blue) voltages for two events passing the selection criteria described in Section 3, in units of the RMS voltage amplitude σ.

However, some events exhibit post-inversion artefacts that appear to be more significant than this, while others do not, as shown in Figure 4 (note the "echoes" of the primary signal offset by exactly 781.25 ns).

The timescale of the fine filterbank artefacts is too long to affect cosmic ray studies, and only acts to slightly increase the noise level. However, the coarse filterbank artefacts limit the precision of automated reconstruction techniques.

4.2 Like cosmic ray events

After the above cuts, 21 events remain. A further test of a cosmic ray origin would be to ensure that their polarisation is consistent with the excess in the $\vec{v} \times \vec{B}$ direction expected from the geomagnetic mechanism, given their reconstructed arrival direction. We could also check that the events arrive preferentially from sensitive regions in the MWA beam. The timing uncertainty discussed above (caused by to PFB artefacts) however translates into a large uncertainty in arrival direction reconstruction, and thus we are limited in our ability to perform these tests.

Figure 5 (left) shows the locations of the remaining 21 events in the array. Three are consistent with low-intensity versions of an unidentified RFI source known to produce events such as that shown in Figure 5 (right), and we reject them. Such RFI events arrived from the North-East close to the horizon. The RFI source is presumably relatively local, as tiles in the North-East were preferentially triggered. A further seven are located in two groups to the North-East of the core area, and are also rejected due to their repeated nature. All ten also have large extents with significant gaps. We cannot fully exclude that 1–2 of these events were genuine cosmic ray events masked by RFI however.

Of the remaining 11, another had its data accidentally deleted, preventing further analysis; while one was detected during a burst of RFI and was surrounded by many impulsive signals. The remaining nine we deem as likely cosmic ray events: they are predominantly East–West polarised, the triggering tiles are in reasonably proximity with no gaps; and their time profiles are impulse-like, with off-pulse structure only at the expected positions for PFB inversion artefacts. Our best event is plotted in Figure 6. It was detected on 17 tiles with arrival direction with the MWA's half-power beam.

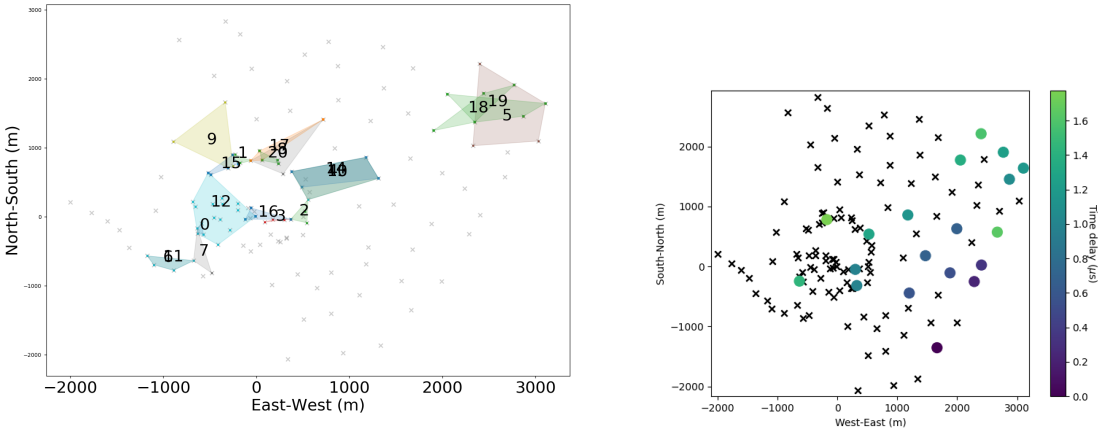

Figure 5: Left: locations of events passing all cuts. The three in the top right clearly resemble low-intensity versions of the RFI shown on the right. Right: example of a typical RFI event, showing the triggered tiles, and the time of arrival.

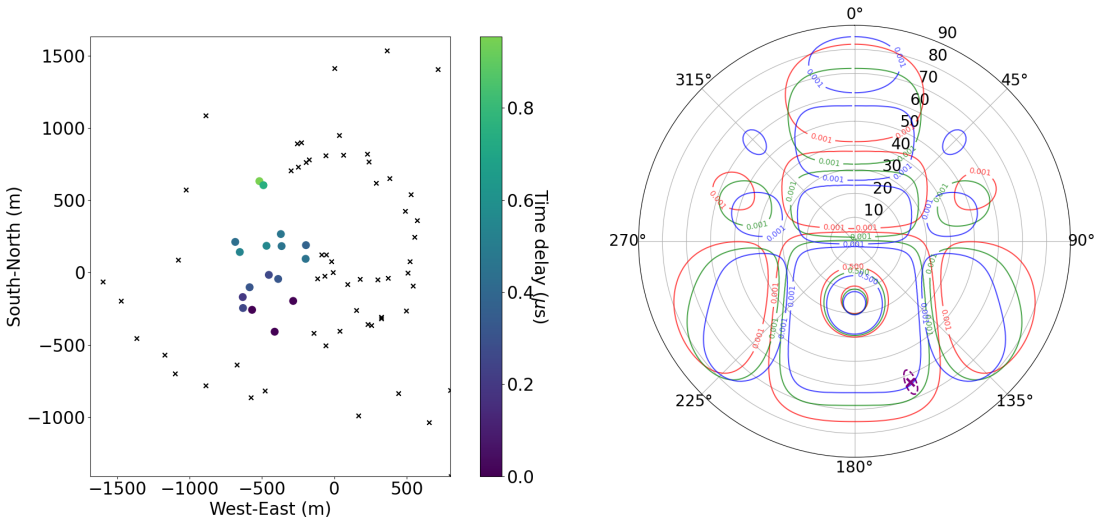

Figure 6: Our best cosmic ray candidate. Left: tiles participating in the coincidence, colour-coded by their relative trigger time; and right: the reconstructed arrival direction (purple), compared to the MWA beam pattern at the bottom (red), middle (green), and top (blue) of the observation band.

5. Discussion/Conclusion

We have processed 26 hr of MWA VCS data, and detected the MWA's first cosmic ray events. Since the array was in extended configuration, and we have significant PFB inversion artefacts, the majority of events do not have sufficiently precise information to classify them as being from cosmic rays or RFI. However, we are confident that we have nine detections, i.e. our minimum detectable rate is $0.34\,\mathrm{hr}^{-1}$.

Importantly, we have encountered a very low RFI rate — of order two events/minute only, when

excluding two periods (less than 10% of the data) with unusually high rates. This is many orders of magnitude lower than encountered with similar experiments at OVRO-LWA [4] and LOFAR [2], and due to the remoteness of, and strict RFI controls within, the MRO.

The next phase of the project is to implement a real-time trigger using an array of particle detectors place near the MWA's centre, and the real-time buffering capability of the MWA's upgraded correlator, which is currently being installed. In particular, we aim to observe in the MWA's compact configuration, where we expect dozens of tiles to trigger on observable events.

ACKNOWLEDGEMENTS This scientific work makes use of the Murchison Radio-astronomy Observatory, operated by CSIRO. We acknowledge the Wajarri Yamatji people as the traditional owners of the Observatory site. Support for the operation of the MWA is provided by the Australian Government (NCRIS), under a contract to Curtin University administered by Astronomy Australia Limited. We acknowledge the Pawsey Supercomputing Centre which is supported by the Western Australian and Australian Governments. CWJ acknowledges support of the Australia Research Council Discovery project DP200102643.

References

[1] T. Huege, *Radio detection of cosmic ray air showers in the digital era*, Phys.Rep. **620**, 1 (2016) [arxiv:1601.07426].

[2] P. Schellart *et al.*, *Detecting cosmic rays with the LOFAR radio telescope*, Astropart.Phys. **560**, A98 (2013) [arxiv:1311.1399].

[3] A. Corstanje *et al.*, *The shape of the radio wavefront of extensive air showers as measured with LOFAR*, Astropart.Phys. **61**, 22 (2015) [arxiv:1404.3907].

[4] R. Monroe *et al.*, *Self-triggered radio detection and identification of cosmic air showers with the OVRO-LWA*, NIMPR A **953**, 163086 (2020) [arxiv:1907.10193].

[5] T. Huege *et al.*, *Precision measurements of cosmic ray air showers with the SKA*, in *Advancing Astrophysics with the Square Kilometre Array*, 148 (2015) [arXiv:1408.5288].

[6] S. J. Tingay *et al.*, *The Murchison Widefield Array: The Square Kilometre Array Precursor at Low Radio Frequencies*, PASA **30**, e007 (2013) [arxiv:1206.6945].

[7] S. E. Tremblay, *et al.*, *The High Time and Frequency Resolution Capabilities of the Murchison Widefield Array*, PASA **32**, e005 (2015).

[8] S. J. McSweeney *et al.*, *MWA tied-array processing III: Microsecond time resolution via a polyphase synthesis filter*, PASA **37**, e034 (2020) [arxiv:2007.03171].

[9] A. Williamson *et al.*, *An Ultra-High Time Resolution Cosmic-Ray Detection Mode for the Murchison Widefield Array*, JAI **10**, 2150003 (2021) [arxiv:2102.04619].